Title : will be set by the publisher
Editors : will be set by the publisher
EAS Publications Series, Vol. ?, 2008

ADAPTED SCALE IMAGE SUBTRACTION FOR ACHROMATIC CORONOGRAPHY

Jean GAY[1], Yves RABBIA[1] and Jean-Pierre RIVET[2]

Abstract. The detection of a faint companion to a star with achromatic coronography and adaptative optics is only limited by the residual speckles. We study a method to increase the detectability of the companion, based on the difference of two images taken in two different wavelengths, after suitable rescaling.

1 Introduction

Adaptative optics devices, which are now available on most astronomical large telescopes, enable diffraction-limited imaging. The images so obtained are only damaged by residual speckles, whose spatial distribution is identical for different wavelengths, provided the wavelength as been chosen as the space scale unit in the focal plane.

This statement laid Racine *et al.* (1999) to propose a method improving the detectability of faint companions. This method involves the subtraction of images taken simultaneously at different wavelengths, after suitable space rescaling. The importance of residual speckles is thereby considerably decreased, and the limiting magnitude of a detectable companion is improved.

However, the efficiency of this method is limited by the stellar photon noise, especially close to the main body of the Airy diffraction spot of the main star. Moreover, the energy subtraction law varies from the center to the border of the image. This makes the exact subtraction over the whole field impossible. To reach sufficient damping of the residual speckles, one thus needs to perform a subtractive combination of three images taken at three different wavelengths.

Coronographic methods, which eliminate or at least damp the stellar contribution, should lead to a better efficiency of this subtractive method, provided the residual speckles at different wavelengths remain similar after their transit through the coronograph. The Achromatic Interferential Coronograph (AIC) (Baudoz

[1] Dept. Fresnel, Observatoire de la Côte d'Azur, B.P. 4229, F-06304 Nice Cedex 4, France
[2] Dept. Cassini, Observatoire de la Côte d'Azur, B.P. 4229, F-06304 Nice Cedex 4, France

DOI: (will be inserted later)

1999; Baudoz *et al.* 2000; Gay & Rabbia 1996a; Gay, Rabbia & Baudoz 1997a) does preserve the similarity of the speckles at different wavelengths. The extinction method proposed by Serabyn (1999) to implement achromatically Bracewell's interferometric nulling concept (1979) should also have this benefic property. The sectored phase mask coronograph proposed by Rouan *et al.* (2000) would also have this property, provided the phase shifts are achromatic, as it is the case for Vakili's implementation (achromatic phase knife coronograph) (Abe *et al.* 2001). In this article, we focus our interest on the AIC, since, contrarily to the other coronographic methods quoted above, this concept has already been implemented and tested on a telescope.

We mention "*en passant*" that the subtraction method can also be applied to simultaneous images taken at the same wavelength, but with two different polarizations. The elimination of the Airy diffraction spot and of the surrounding speckles is accurate, even without adaptative optics. A faint companion should emerge if its light is strongly polarized (Seagers *et al.* 2000), and if the polarization plane of the instrument has the right orientation with respect to the *a priori* unknown direction of the observed binary system. The latter condition requires to try at least three orientations of the instrument. However, without coronography, the method remains limited by the photon noise of the main star, and is only sensitive to the light diffused by the companion, which is dominated by short wavelengths. Moreover, the polarization rate varies rapidly with the phase of the companion, and reaches its maximum at quadratures. This is a limitation to the observable period of the binary system. This is however a promising method to measure the albedo of giant exo-planets.

2 Principles of the AIC

In its initial version (Baudoz 1999; Baudoz *et al.* 2000; Gay & Rabbia 1996a; Gay, Rabbia & Baudoz 1997a), the Achromatic Interferential Coronograph (AIC) is a Michelson interferometer, one arm of which includes an afocal device with a focus crossing, so that the light passing through this arm is achromatically phase-shifted of π, and reversed (see Figure 1). The optical path difference between both arms is tuned to zero, so that the light of a star exactely on the axis of the afocal device (thus invariant by reversal), will vanish by destructive interference when recombined at the output of the interferometer. A companion which is not on this extinction axis will lead to two images with identical intensity, and symmetric with respect to the extinction axis (see Figure 2). It is worth noting that if the separating plate of the Michelson interferometer is well balanced ($R = T = 0.5$), each of these two images gather only one quarter of the total collected energy. Thus, only one half of the companion photons is available at the output. The fact that any off-axis point leads to two symmetrical images erases any asymmetry in the image of the neighborhood of the star. This may be a drawback for a star with an envelope since the latter would not be correctly rendered if asymmetric. For a star with a single companion however, this symmetrization is harmless. It may even be benefic for astrometry, since an orbital motion would emerge with twice

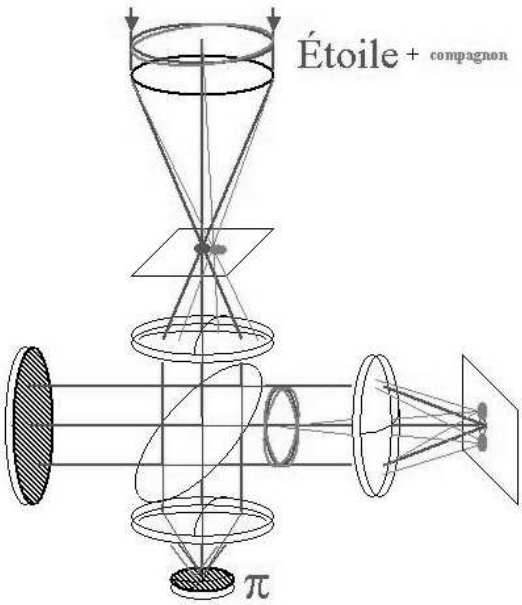

Fig. 1. The principle of the AIC. To ease the understanding of this picture, the afocal system is represented by a lens and a curved mirror. In the real implementation, only mirrors are used, to avoid chromatic aberrations. Black rays and wave fronts : the light of the main star. Grey rays and wave fronts : the light of the companion.

less observation time.

In what follows, we express the wave amplitudes in the pupil plane as functions of normalized coordinates :

$$\mathbf{r} = (x, y) = (r\cos\phi, r\sin\phi), \tag{2.1}$$

rescaled by the radius of the telescope entrance aperture, with the origin at the center of the aperture. For amplitudes in the image plane, we use angular coordinates on the sky (see Figure 3) :

$$\mathbf{\Theta} = (\alpha, \beta) = (\theta\cos\chi, \theta\sin\chi). \tag{2.2}$$

The transmission function $\Pi(\mathbf{r})$ of the pupil is assumed to be invariant under central symmetry :

$$\Pi(-\mathbf{r}) = \Pi(\mathbf{r}). \tag{2.3}$$

The effect of atmospheric turbulence partially corrected by the adaptative optics (see Figure 4) is modeled by a wave front distortion, that is, by a phase shift $\Phi(\mathbf{r})$ in the pupil plane, so that the complex transmission function of the pupil reads :

$$P(\mathbf{r}) = \Pi(\mathbf{r})e^{i\Phi(\mathbf{r})}. \tag{2.4}$$

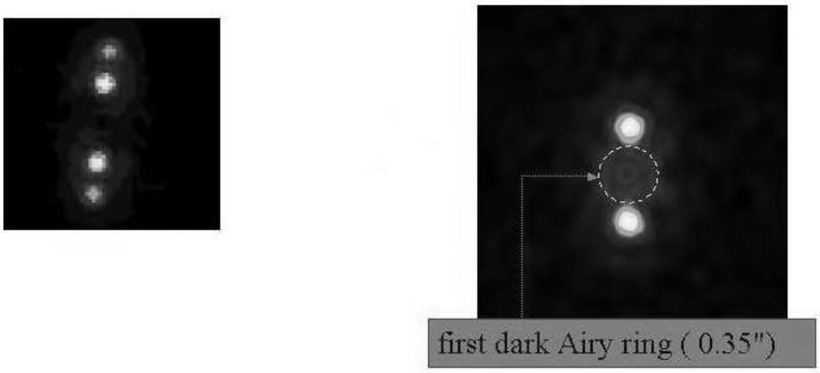

Fig. 2. First test of the AIC on the $1.5\,m$ telescope of the "Observatoire de Haute Provence" (France), with ONERA adaptative optics and STSci camera in K-band. The binary system observed was $72 - Peg$ ($\Delta m_k = 0.36$, $\rho = 0.53''$). Left image : the main star is off-axis with respect of the coronograph. Right image : the main star is on-axis.

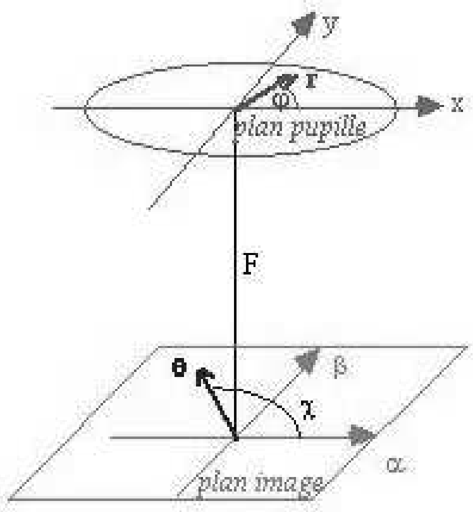

Fig. 3. The two systems of normalized coordinates for points in the pupil plane and in the image plane.

Let us now introduce the properties of the beam splitter. R and T denote respectively its reflection and transmission coefficients for the energy. The reflection and transmission coefficients for the amplitude are respectively :

$$\rho = \sqrt{R}e^{i\mu} \quad \text{and} \quad \tau = \sqrt{T}e^{i\nu}, \tag{2.5}$$

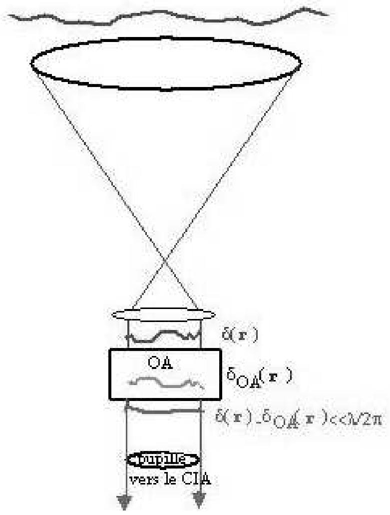

Fig. 4. An illustration of a wave front distorted by turbulence, and its partial correction by the adaptative optics device.

where the phases and the amplitudes must satisfy :

$$R + T = 1 \quad \text{and} \quad \mu - \nu = \frac{\pi}{2} + k\pi, \tag{2.6}$$

for and ideal beam splitter without absorption.

Consider a star in the direction Θ, and a band of wave lengths ranging from $\lambda - \delta\lambda/2$ to $\lambda + \delta\lambda/2$. At the output of the AIC, the amplitude in this band of wavelengths in the pupil plane is :

$$A_{\Theta,\lambda}(\mathbf{r}) = \rho\tau\big(P(\mathbf{r})e^{i\frac{2\pi}{\lambda}\Theta\cdot\mathbf{r}} - P(-\mathbf{r})e^{-i\frac{2\pi}{\lambda}\Theta\cdot\mathbf{r}}\big)\sqrt{S(\lambda,\theta)\delta\lambda}\,. \tag{2.7}$$

Here, $S(\lambda, \theta)$ is the spectral density of light flux incoming from the star in direction Θ. If the star is off-axis, the total power available at the output of the AIC in the spectral band $\delta\lambda$ is :

$$W(\lambda, \Theta) = 2RT.\Sigma.S(\lambda, \theta)\delta\lambda, \tag{2.8}$$

where $\Sigma = \int \Pi(\mathbf{r})d^2\mathbf{r}$ is the area of the aperture of the collecting telescope.

3 Approximation for weak residual deformations of the wave front

If turbulence is not taken into account, the amplitude distribution in the spectral band $\delta\lambda$ in the image (focal) plane can be expressed in terms of $\tilde{\Pi}$, the Fourier transform of the pupil transmission function :

$$A_{\Theta,\lambda}(\mathbf{\Gamma}) = \frac{\rho\tau}{i\lambda}\big(\tilde{\Pi}(\frac{\Gamma - \Theta}{\lambda}) - \tilde{\Pi}(\frac{\Gamma + \Theta}{\lambda})\big)\sqrt{S(\lambda, \theta)\delta\lambda}. \tag{3.1}$$

Γ denotes the vector-position of a point in the image plane. The distribution of light intensity follows immediately :

$$E_{\Theta,\lambda}(\mathbf{\Gamma}) = \frac{RT}{\lambda^2}\big(\tilde{\Pi}(\frac{\Gamma-\Theta}{\lambda}) - \tilde{\Pi}(\frac{\Gamma+\Theta}{\lambda})\big)^2 S(\lambda,\theta)\delta\lambda. \tag{3.2}$$

This distribution vanishes if $\Theta = \mathbf{0}$, that is, when the star is on the extinction axis of the AIC. (in the sequel, the quantities related to the central star on-axis will be labeled with the index "$\star$"). When the star is on the axis, the effect of residual turbulence cannot be neglected anymore, and the phase shift $\Phi(\mathbf{r})$ must be incorporated. For further convenience, let us introduce the optical path fluctuation $\delta(\mathbf{r})$ corresponding with the phase shift $\Phi(\mathbf{r})$:

$$\delta(\mathbf{r}) \equiv \frac{\lambda}{2\pi}\Phi(\mathbf{r}). \tag{3.3}$$

The amplitude distribution in the pupil plane now reads :

$$A_{\star,\lambda}(\mathbf{r}) = \rho\tau\big(\Pi(\mathbf{r})e^{i\frac{2\pi}{\lambda}\delta(\mathbf{r})} - \Pi(-\mathbf{r})e^{i\frac{2\pi}{\lambda}\delta(-\mathbf{r})}\big)\sqrt{S_\star(\lambda)\delta\lambda}. \tag{3.4}$$

$S_\star(\lambda)$ is the spectral density of light flux of the central star

If the adaptative optics device is efficient enough to bound the residual phase shift $\Phi(\mathbf{r})$ below a value much smaller than one, then the exponentials can be expanded in powers of $\Phi(\mathbf{r})$. Taking into account the symmetry of the pupil transmission function $\Pi(\mathbf{r}) = \Pi(-\mathbf{r})$, Equation (3.4) reduces to :

$$A_{\star,\lambda}(\mathbf{r}) \simeq \rho\tau\frac{2\pi i}{\lambda}\Pi(\mathbf{r})\big(\delta(\mathbf{r}) - \delta(-\mathbf{r})\big)\sqrt{S_\star(\lambda)\delta\lambda}. \tag{3.5}$$

The antisymmetric part $\Delta(\mathbf{r}) \equiv \Pi(\mathbf{r})\big(\delta(\mathbf{r}) - \delta(-\mathbf{r})\big)/2$ of the turbulent aberration emerges naturally in (3.5). Its Fourier transform $\tilde{\Delta}(\mathbf{f})$ is imaginary and antisymmetric. We thus introduce the odd real function $D(\mathbf{f})$ such that :

$$\tilde{\Delta}\mathbf{f} = i\,D(\mathbf{f}). \tag{3.6}$$

The amplitude distribution in the image plane is then :

$$A_{\star,\lambda}(\Gamma) \simeq \frac{4\pi}{\lambda^2}\rho\tau D(\frac{\Gamma}{\lambda})\sqrt{S_\star(\lambda)\delta\lambda}, \tag{3.7}$$

and the corresponding light flux distribution is :

$$E_{\star,\lambda}(\Gamma) \simeq \frac{4\pi^2}{\lambda^4}(4RT)D^2(\frac{\Gamma}{\lambda})S_\star(\lambda)\delta\lambda. \tag{3.8}$$

This is the expression of the energy distribution in the image plane of the residual speckle pattern of the main star (on-axis), at the output of the AIC, in the limit of small phase shifts ($|\Phi(\mathbf{r})| << 1$).

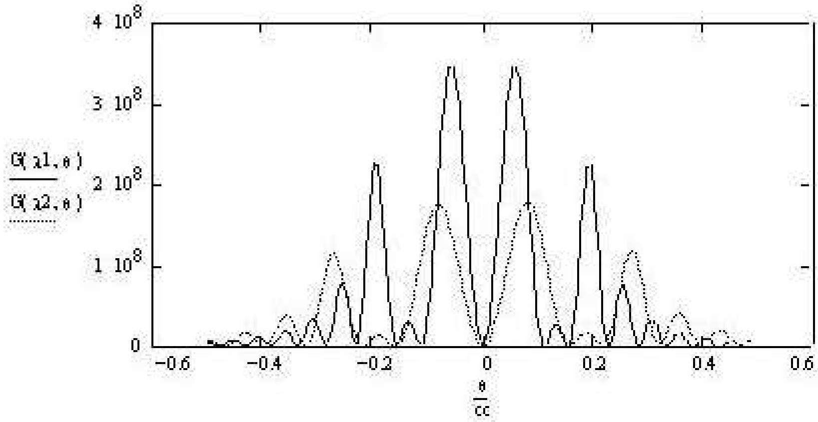

Fig. 5. A cut along a straight line through two simulated speckle patterns at two different wavelengths. The similarity of both curves is visible.

4 The adapted scale subtraction

The residual speckles appear clearly in Equation (3.8) to be homothetic for different wavelengths. However, space rescaling is not sufficient to make speckles at different wavelength identical. A rescaling of the energy is also required. To do so, let us introduce $\omega_\star(\lambda)$, the total residual energy in the image plane at the output of the AIC, in the spectral band considered :

$$\omega_\star(\lambda) = \int E_{\star,\lambda}(\Gamma) d^2\Gamma. \tag{4.1}$$

This total residual energy is related to Δ_{rms}, the root mean square of the anti-symmetric part $\Delta(\mathbf{r})$ of the optical path fluctuation :

$$\frac{\omega_\star(\lambda)}{\Sigma} = 4RT\,(\frac{2\pi\Delta_{rms}}{\lambda})^2 S_\star(\lambda)\delta\lambda. \tag{4.2}$$

This yields a to an expression for the light flux distribution, where both the spatial and the energy scaling appear clearly :

$$E_{\star,\lambda}(\Gamma) \simeq \frac{\omega_\star(\lambda)}{\lambda^2\Sigma} D^2(\frac{\Gamma}{\lambda}). \tag{4.3}$$

Figure 5 shows a cut along a straight line through a simulated speckle pattern a two different wavelengths. The dashed curve can be superposed to the solid one by a space and energy rescaling. Under the form (4.3), the subtraction of two speckle patterns at wavelengths λ_1 and λ_2 leads to a vanishing contribution :

$$\frac{\lambda_1^2}{\omega_\star(\lambda_1)}\; E_{\star,\lambda_1}(\Gamma\lambda_1) - \frac{\lambda_2^2}{\omega_\star(\lambda_2)}\; E_{\star,\lambda_2}(\Gamma\lambda_2) = \mathcal{O}(|\Phi(\mathbf{r})|^2), \tag{4.4}$$

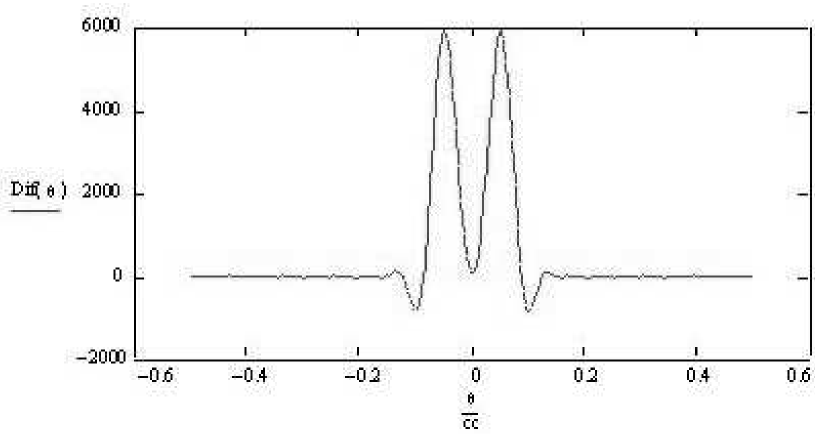

Fig. 6. A faint companion emerges out of this cut through a simulated image, after the residual speckles have been removed by adapted scale subtraction.

at least in the limit where the residual turbulent phase shift $\Phi(\mathbf{r})$ is small enough to make terms of order $|\Phi(\mathbf{r})|^2$ irrelevant.

The total residual energy $\omega_\star(\lambda)$ due to the main star can be computed by integration of the energy present in the image plane, only if the contribution of the companion is negligible. This is actually the case in coronography. Indeed, if a companion is bright enough to contribute significantly to the total energy in the image plane, then, no coronograph is needed.

To take advantage of this possibility to eliminate the speckles of the main star, we use two simultaneous images $E_{\lambda_0}(\Gamma)$ and $E_\lambda(\Gamma)$ obtained in two spectral bands around λ_0 and λ respectively. Then, we propose to compute the following quantity :

$$\begin{aligned} \sigma_{\lambda_0,\lambda}(\Gamma) &= E_{\lambda_0}(\Gamma) - E_\lambda(\Gamma\tfrac{\lambda}{\lambda_0}) \times \tfrac{\omega_\star(\lambda_0)}{\omega_\star(\lambda)}\left(\tfrac{\lambda}{\lambda_0}\right)^2 \\ &= E_{\lambda_0}(\Gamma) - E_\lambda(\Gamma\tfrac{\lambda}{\lambda_0}) \times \tfrac{S_\star(\lambda_0)\delta\lambda_0}{S_\star(\lambda)\delta\lambda}\left(\tfrac{\lambda}{\lambda_0}\right)^4 \end{aligned} . \qquad (4.5)$$

To obtain the second expression, in terms of $S_\star(\lambda)$, we have used Equation (4.2). As a consequence of (4.4), the contribution of the main star to $\sigma_{\lambda_0,\lambda}(\Gamma)$ vanishes, in the limit of small residual phase shifts.

We consider now a faint companion in direction Θ. Its image at the output of the AIC, after the adapted scale subtraction operation has been performed, is :

$$\sigma_{\Theta,\lambda_0,\lambda}(\Gamma) = E_{\Theta,\lambda_0}(\Gamma) - E_{\Theta,\lambda}(\Gamma\frac{\lambda}{\lambda_0}) \times \frac{S_\star(\lambda_0)\delta\lambda_0}{S_\star(\lambda)\delta\lambda}\left(\frac{\lambda}{\lambda_0}\right)^4 \qquad (4.6)$$

This expression can be written in terms of the differences of magnitudes between the companion and the main star, in the two spectral bands:

$$\Delta m = 2.5 \log_{10} \left(\frac{S_\star(\lambda)}{S(\lambda,\Theta)} \right) \qquad \text{and} \qquad \Delta m_0 = 2.5 \log_{10} \left(\frac{S_\star(\lambda_0)}{S(\lambda_0,\Theta)} \right), \tag{4.7}$$

and of the distribution:

$$M_\lambda(\Gamma,\Theta) = \big(\tilde{\Pi}(\frac{\Gamma-\Theta}{\lambda}) - \tilde{\Pi}(\frac{\Gamma+\Theta}{\lambda}) \big)^2. \tag{4.8}$$

The resulting expression reads:

$$\begin{aligned} \sigma_{\Theta,\lambda_0,\lambda}(\Gamma) = {} & \tfrac{RT}{\lambda_0^2} S_\star(\lambda_0)\delta\lambda_0 \times \\ & \left(10^{-0.4\Delta m_0} M_{\lambda_0}(\Gamma,\Theta) - \left(\tfrac{\lambda}{\lambda_0}\right)^2 10^{-0.4\Delta m} M_\lambda(\Gamma\tfrac{\lambda}{\lambda_0},\Theta) \right). \end{aligned} \tag{4.9}$$

Since $M_\lambda(\Gamma\frac{\lambda}{\lambda_0},\Theta) = M_{\lambda_0}(\Gamma,\Theta\frac{\lambda_0}{\lambda})$, the contribution of the companion is:

$$\begin{aligned} \sigma_{\Theta,\lambda_0,\lambda}(\Gamma) = {} & \tfrac{RT}{\lambda_0^2} S_\star(\lambda_0)\delta\lambda_0 10^{-0.4\Delta m_0} \times \\ & \left(M_{\lambda_0}(\Gamma,\Theta) - \left(\tfrac{\lambda}{\lambda_0}\right)^2 10^{-0.4(\Delta m-\Delta m_0)} M_{\lambda_0}(\Gamma,\Theta\tfrac{\lambda_0}{\lambda}) \right). \end{aligned} \tag{4.10}$$

Figure 6 shows the result of the adapted scale subtraction method applied to the two one-dimensional simulated speckle patterns in Figure 5. The speckles are eliminated, and a faint companion emerges.

Up to a photometric multiplicative factor, the image resulting from the adapted scale subtraction method depends on the discrepancy between the magnitude differences in the two spectral bands under consideration. The distribution $M_\lambda(\Gamma,\Theta)$ is characteristic of AIC images. It is symmetric with respect to the center of extinction, and displays two distinct bright spots at $\Gamma = \pm\Theta$ if the separation θ is larger than the first dark Airy ring. Otherwise, the two spots almost merge and takes the appearance of a pair of "bean-like" structures.

Figure 7 is a graphical summary of the adapted scale subtraction procedure. The results of this method, applied to simulated images, appears in Figure 8. The individual images differ by the details of the turbulent wave front distortion, but obey to the same statistics. The Strehl ratio for the first wavelength $\lambda_0 = 3.5$ is 0.90. For the second wavelength $\lambda = 4.9$, it reaches 0.96.

5 The limitations

We only mention these limitations, and postpone to a further publication the detailed study of their influence on the efficiency of the method.

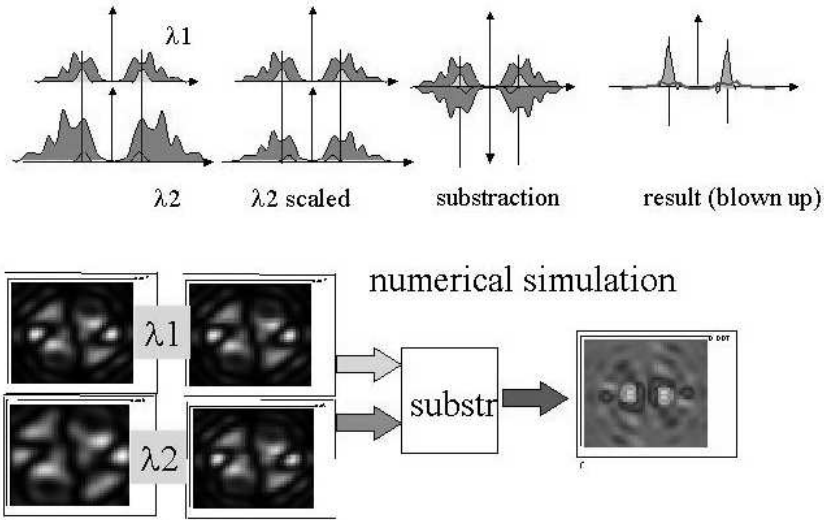

Fig. 7. A graphic illustration of the adapted scale subtraction method.

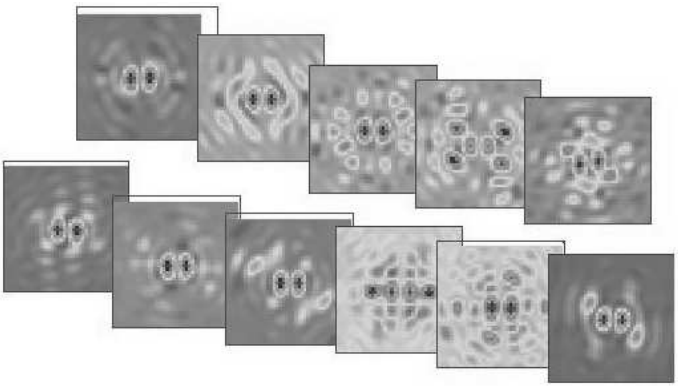

Fig. 8. test

5.1 The validity of the expansion

We have assumed that the expansion at the first order in the optical path turbulent fluctuation could render correctly the reality. The contribution of the second order terms should be studied. They involve the even part of the wave front distortion:

$$\Omega(\mathbf{r}) = \frac{1}{2}\Pi(\mathbf{r})\big(\delta(\mathbf{r}) + \delta(-\mathbf{r})\big).$$

On can show that it contributes by fourth order corrections to the residual light flux distribution. It vanishes near the center of the field, but spreads over the remainder of the field. A rapid estimate shows that it leads to a very smooth background, ten magnitudes below the level of the off-axis star, for the conditions of the simulation in Figure 8.

5.2 Spectral decorrelation of the turbulence

This problem, that merely affects high space frequencies, is only relevant relatively far from the extinction center. The origin of this phenomenon is to be found in the chromaticity of Fresnel's propagation through the atmospheric layers. Simulations performed by Carbillet *et al.* (2002) show that its consequences are even weaker than those of the aforementioned limitation.

In the case of a space telescope, the wave front distortions are rigorously achromatic, since they originate from the mirror defects only.

5.3 Misalignments

The theory presented in this article assumes that the pupil of the telescope is invariant under central symmetry. This is only the case if the mechanical positions and orientations of the optical elements in the AIC is such that the axis of extinction runs exactly through the center of the telescope pupil. Achieving this condition is one of the major difficulties in the implementation of the AIC.

6 The implementation

A compact implementation of the AIC concept has been designed and realized. It has been running on the the $3.6\,m$ Canada-France Hawaiian Telescope (CFHT). It delivers simultaneously two coronographic images in the sub-bands K_1 and K_2 of the K band ($2.1\,\mu m$ and $2.3\,\mu m$). The K_1 band is outside of the methane absorption lines, whereas K_2 encompasses them completely. The long term purpose of this choice is the detection of methane, which is expected in the atmosphere of giant exo-planets.

Figure 9 shows a schematic diagram of the compact AIC designed for CFHT. The afocal arm of the Michelson interferometer is visible on the left side. the neutral arm (without focus crossing) appears on the right side. Figure 10 is a photograph of the AIC (highlighted inside the white rectangle), and of its surrounding optics. The keys have been put on top of it, just to give the scale of the photograph. Figure 11 is a coronographic image of the binary star $HIP97339$ recorded at CFHT. The dotted circle highlights the first dark Airy ring. The companion appears under the "bean-like" shape, since the separation ($0.13''$) is below the Airy radius at $2.2\,\mu m$ ($0.15''$).

7 Conclusion

Simultaneous imaging at several (at least two) wavelengths through an AIC with adapted scale image subtraction should increase of about ten magnitudes the extinction capabilities of the AIC itself. However, this technique has to be validated

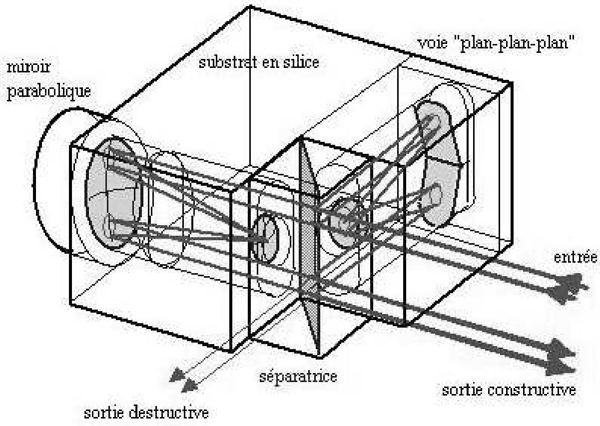

Fig. 9. A perspective view of the AIC in the configuration tested on the 3.6m Canada-France Hawaiian Telescope (CFHT).

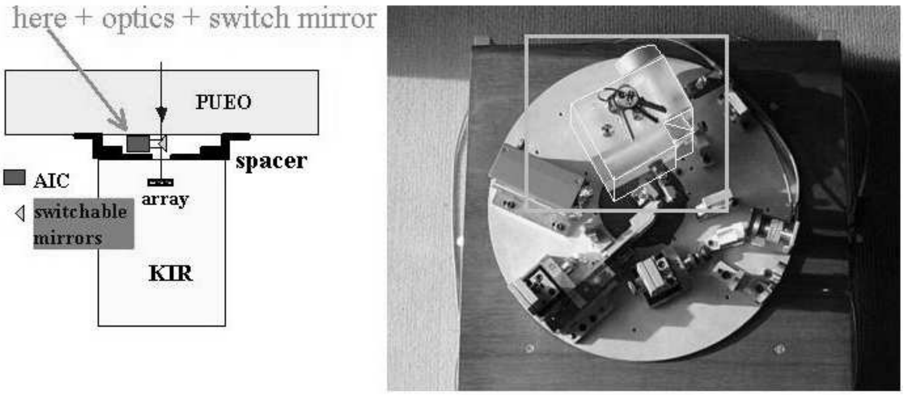

Fig. 10. Left : The AIC in the spacer between the PUEO adaptative optics and the KIR infrared camera at CFH. Right : a photograph of the AIC and of its surrounding optics, ready to be inserted in the spacer.

and evaluated quantitatively on the real astronomical images taken during the four observation runs already performed at CFHT.

References

Abe, L., Vakili, F. & Boccaletti, A. 2001 *A&A*, **374**, pp. 1161–1168.

Baudoz, P. 1999, *"Coronographe Interférentiel achromatique"*, PhD Thesis, Nice (France).

Baudoz, P., Rabbia, Y. & Gay, J. 2000, *A&AS*, **141**, pp. 319–329.

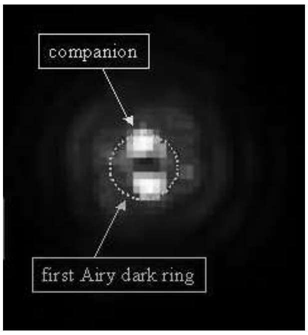

Fig. 11. A coronographic image of $HIP\,97339$ ($M = 8$, Type=$B9$). Separation : $\rho = 0.13''$. Radius of the first Airy dark ring : $0.15''$. Exposure time : 15 *sec.* Number of frames : 20. Seeing : $1.4''$.

Bracewell, R.N. & Mc Phie, R.H. 1979, *Icarus*, **38**, pp. 138-147.

Gay, J. & Rabbia, Y. 1996, *C. R. Acad. Sci. Paris IIb*, **322**, pp. 265–271.

Gay, J. & Rabbia, Y., & Baudoz, P. 1997, *C. R. Acad. Sci. Paris IIb*, **325**, pp. 51–56.

Racine, R., Walker, G., Nadeau, D., Doyon, R. & Marois, C. 1999, *PASP*, **111**, pp. 587–594.

Rouan, D., Riaud, P., Boccaletti, A., Clénet, Y. & Labeyrie, A. 2000, *PASP*, **112**, pp. 1479–1486.

Seagers, @. *et al.*2000, *ApJ*, **540**(1), pp. 504–520.

Serabyn, E. *et al.* 1999, *Appl. Optics*, **38**(34), pp 7128–7132.